Local topography increasingly influences the mass balance of a retreating cirque glacier

Caitlyn Florentine[1,2], Joel Harper[1], Daniel Fagre[2], Johnnie Moore[1], Erich Peitzsch[2]

[1]Department of Geosciences, University of Montana, Missoula, Montana, 59801, USA
5 [2]U.S. Geological Survey, Northern Rocky Mountain Science Center, West Glacier, Montana, 59936, USA

Correspondence to: Caitlyn Florentine (caitlyn.florentine@umontana.edu)

10 **Abstract.** Local topographically driven processes such as wind drifting, avalanching, and shading, are known to alter the relationship between the mass balance of small cirque glaciers and regional climate. Yet partitioning such local effects apart from regional climate influence has proven difficult, creating uncertainty in the climate representativeness of some glaciers. We address this problem for Sperry Glacier in Glacier National Park, USA using field-measured surface mass balance, geodetic constraints on mass balance, and regional climate data recorded at a network of meteorological stations.

15 Geodetically derived mass changes between 1950-1960, 1960-2005, and 2005-2014 document average mass loss rates during each period at -0.22±0.12 m w.e. yr^{-1}, -0.18±0.05 m w.e. yr^{-1}, and -0.10±0.03 m w.e. yr^{-1}. A correlation of field-measured mass balance and regional climate variables closely predicts the geodetically measured mass loss from 2005-2014. However, this correlation overestimates glacier mass balance for 1950-1960 by +1.18±0.92 m w.e. yr^{-1}. This suggests that local effects, not represented in regional climate variables, have become a more dominant driver of the net mass balance as

20 the glacier lost 0.50 km^2 and retreated further into its cirque.

1 Introduction

Glaciers are sensitive indicators of climate (Dyurgerov and Meier, 2000; Roe et al., 2016; Zemp et al., 2015) because ice mass gains are ultimately controlled by winter precipitation, and ice mass losses are ultimately controlled by radiation inputs during summer. However, prior studies of small mountain glaciers show that local topographic effects, including

25 avalanching, wind drifting, and shading, enhance winter mass gains or mediate summer mass losses (e.g. Hock, 2003; Kuhn, 1995; Laha et al., 2017). These topographically driven mass balance processes complicate the relationship between regional climate and cirque glacier surface mass balance.

Such complications have been documented with the small glaciers of the North American Rocky Mountains. In Colorado, glacier mass balance showed no statistically significant relationship to variations in winter precipitation during the 20th century (Hoffman et al., 2007). This result implied the importance of processes driven by local topography, including snow avalanching and wind drifting. In the Canadian Rockies, an inventory of nearly 2,000 glaciers showed that while larger

5   glaciers retreated during the last half of the 20th century, very small glaciers did not change (DeBeer and Sharp, 2007). A follow-up analysis showed that the stability of these very small (<0.4 km^2) glaciers was closely related to their topographically favorable setting (DeBeer and Sharp, 2009).

Since local topography can substantially influence the mass balance of small and sheltered mountain glaciers, it follows that as glaciers retreat further toward cirque headwalls, the direct control of regional climate on glacier mass balance should

10   diminish, and local processes should become more influential. That said, Andrews Glacier in Colorado exhibited a strong correlation (r = -0.93) between summer temperature and net annual balance (Hoffman et al., 2007), despite enhanced accumulation via wind drifting and avalanching during the winter: the mass losses during summer outweighed the extra snow provided by topographically driven snow redistribution. Regional climate can therefore remain the primary driver of net mass balance, even when local topography plays a strong role.

15   This paper examines the time evolution of the partitioning between regional climate and local influences on glacier mass balance of a glacier retreating into its cirque. Since 1966, Sperry Glacier, Montana has reduced in area by 40% and retreated hundreds of meters (Fagre et al., 2017). We hypothesize that during a recent interval (2005-2014), as a larger proportion of the glacier surface has become sheltered by its cirque headwall, the relationship between specific mass balance and regional climate is quantifiably distinct from that during mid-century (1950-1960), when the glacier extended further downslope from

20   its cirque headwall. We leverage relatively unique observations to test this hypothesis, including a field measured (glaciological) surface mass balance record and repeat geodetic mass balances.

2 Study area

Sperry Glacier sits just west of the Continental Divide, occupying a cirque that abuts the 2,801 m high Gunsight Peak, and is roughly in the center of Glacier National Park (GNP), Montana (Fig. 1a). A bedrock headwall, crested by a ridgeline that

25   runs 2 km toward the northeast from Gunsight Peak (Fig. 1b), rises 100-300 m above Sperry Glacier (Fig. 2). This headwall is 0.17 km^2 in area, and has slopes between 50° to near vertical. A sub-ridge extends 500 m toward the north, bordering the glacier's western margin (Fig. 1b). Between the headwall and this sub-ridge, Sperry Glacier has a 40° ramp extending to the top of Gunsight Peak, so that some ice overlaps the ridge (Fig. 1b). A cornice that can be 10-20 m high develops every winter along this topmost section of the glacier (Fig. 2). A distinctive bergschrund separates the top 50-150 m of the glacier

30   from the main ice body (Fig. 2). The terrain in front of Sperry Glacier is relatively low angle (<15°).

Moraines located 1 km from the ice terminus (Fig. 2) indicate that in the geologically recent past, the glacier covered most of a topographic bench now bare of ice. These moraines were likely deposited when the glacier was at its Little Ice Age maximum extent (Carrara, 1989). Historical photographs (Alden, 1914; Carrara, 1989) show ice once covered 3.24 km^2. Since that time Sperry Glacier has steadily retreated, decreasing in area to 1.58 km^2 in 1938 (Johnson, 1980), and to 0.80 km^2 in 2015 (Fagre et al., 2017).

3 Methods

3.1 Elevation data

Modern Digital Elevation Models (DEMs) of Sperry Glacier and adjacent terrain were derived from National Technical Means (NTM) imagery collected in 2005 and 2014 (Fahey, 2014). Both images were collected in September, when glacier mass is at an assumed annual minimum, on 02 September 2005 and 07 September 2014 respectively. The DEMs were generated with SOCET SET® software, which uses photogrammetric methods to extract terrain data from imagery (Zhang, 2006). Grid cell resolution was 5 m. The absolute accuracy of the DEM with respect to an independent vertical datum was 3.05 m in the horizontal and 7.54 m in the vertical. The precision of the DEM was 0.44 m and 0.47 m in the horizontal and vertical respectively.

USGS topographic maps at 6.1 m (20 ft) contour resolution were available for Sperry Glacier for 1950 and 1960 (Johnson, 1980). These maps were originally created using aerial photography and Kelsh plotter techniques, guided by 13 plane table bench marks. Both maps document elevation near the assumed September glacier mass minimum, on 01 September 1950 and 08 September 1960. We digitized these historic elevation data by first manually tracing scanned maps to produce digitized contours, and then interpolating digitized contours using a natural neighbor interpolation tool (ESRI, 2014; Sibson, 1981). Grid cell resolution was 5 m. We found that the historic elevation data from the original Johnson (1950, 1960) maps were 56 m lower than the modern vertical datum (EGM96) due to the authors' sea level datum assumption. We remedied this error by adding 56 m to the 1950 and 1960 DEMs.

3.2 Geodetic mass balance and DEM co-registration

The 1950 and 1960 DEMs did not require co-registration since they were originally mapped using a common vertical datum and spatial reference frame. We co-registered the 2005 and 2014, and the 1960 and 2005, DEMs following universal co-registration methods outlined by Nuth and Kääb (2011). The method used a statistical approach that minimized vertical differences over stable, vegetation-free, snow-free, and low-sloping ($< 30^0$) bedrock. After co-registration, the root mean squared error of elevation differences over stable bedrock improved from 8.43 m to 6.91 m for the 1960 and 2005 DEMs, and from 2.48 m to 2.01 m for the 2005 and 2014 DEMs. The mean of bedrock elevation differences after co-registration was effectively zero, i.e. $< 10^{-15}$ m, but differences over individual pixels still ranged from -42 m to +83 m for the 1960 and

2005 DEMs and -15 to +14 m for the 2005 and 2014 DEMs (Fig. S1, Supplement). These large differences tended to occur over steep terrain, and are included in our elevation error estimate.

Glacier margin data for 2005 and 2014, used to clip DEMs to glacier extent, were derived from aerial imagery and ground-based GPS surveys of the glacier terminus. We defined 1950 and 1960 glacier margin data by digitally tracing the glacier

5   from the same historic topographic maps by Johnson (1980).

We generated a record of geodetic mass balance for Sperry Glacier, given by

$$B_a = \frac{\Delta V}{A_{t_1}}\left(\frac{\rho_i}{\rho_w}\right),$$ (1)

where B_a is the specific surface mass balance expressed in meters of water equivalent, ΔV is the change in glacier volume (determined from DEM data described in Sect. 3.1), ρ_i is the density of ice, ρ_w is the density of water (1000 kg m^{-3}), and A_{t_1}

10   is the initial glacier area. To convert volume to mass, we adopted the approximation outlined by Huss (2013), and assigned ice density as $\rho = 850 \pm 60$ kg m^{-3}. Note that this differs somewhat from the 874 kg m^{-3} used for Sperry Glacier glaciological mass balance by Clark et al. (2017), but that this value falls within the uncertainty bounds of our assigned ice density of 850 $\pm$ 60 kg m^{-3}.

3.3 Geodetic mass balance assessment

15   There are three main sources of uncertainty in our geodetic mass balance calculation: elevation errors which affect the volume calculation, density errors which affect the volume to density conversion, and map coverage errors which affect the historic geodetic mass balance.

3.3.1 Elevation change uncertainty

After co-registering DEMs, elevation error on the geodetic mass balance was estimated by analyzing elevation differences

20   over stable bedrock terrain. Since error tends to be greater over steep terrain at high elevations, we analyzed error by elevation band, rather than in bulk across the entire DEM. We used standard error propagation, as applied in previous geodetic mass balance studies (Ruiz et al., 2017; Thomson et al., 2017), given by:

$$E\Delta h_i = \frac{\sigma_{dh}}{\sqrt{N_{eff}}},$$ (2)

where $E\Delta h_i$ is the mean elevation error for a 50 m elevation band (*i*) that spans the glacier, σ_{dh} is the standard deviation of

25   elevation differences over stable bedrock for the elevation band, and N_{eff} is the number of independent values within the elevation band. This in turn is given by:

$$N_{eff} = \frac{N_{tot} \cdot P}{2 \cdot d} \tag{3}$$

where N_{tot} is the total number of pixels (grid cells), P is pixel size, and d is the distance of spatial autocorrelation (100 m), estimated from variogram analysis. We then summed elevation error across the glacier surface, weighting the error by the ratio of the glacier surface covering that elevation band.

3.3.2 Density uncertainty

We followed the convention outlined by Huss (2013) and used a constant density of ρ_i= 850±60 kg m^{-3} to convert glacier volume change to mass, which was derived from a suite of empirical firn densification experiments, and is appropriate for geodetic mass balance calculations where the time intervals considered are longer than 5 years, the volume change is nonzero, and the mass balance gradient is stable. These conditions are satisfied for Sperry Glacier since (a) geodetic mass balance periods are 10 year (1950-1960), 45 year (1960-2005), and 9 year (2005-2014) long, (b) glacier volume changes were nonzero, and (c) glaciological measurements show that mass balance gradients were relatively constant during 2005-2014, i.e. 0.004-0.019 m w.e. m^{-1} for winter and 0.003-0.011 m w.e. m^{-1} for summer (Clark et al., 2017). The ±60 kg m^{-3} density error amounted to <8% error on geodetic mass balances.

We assumed that elevation and density errors were independent, and therefore summed them quadratically to solve for the total error on the geodetic mass balance, given by:

$$E_t = \sqrt{E\Delta h^2 + E\rho^2} \tag{4}$$

where $E\Delta h$ is elevation error, $E\rho$ is density error, and E_t is the total error in m w.e. on the geodetic mass balance.

3.3.3 Map coverage errors

The historic maps used to derive 1950 and 1960 DEMs are missing the upper section of the glacier. Historic photos verify that in the mid-20th century Sperry Glacier extended to the top of Gunsight Peak, as it does today. To enable consistent geodetic mass balance calculation for the entirety of Sperry Glacier, we filled in elevation change over this missing section using modern 2005-2014 results. We opted for this remedy, rather than the alternative of truncating 2005-2014 data, in order to be consistent with glaciological data, which were generated for the entire glacier surface including the upper section. By using modern results to infill missing historic data, we assumed that the rate of mass change in that area near the cirque headwall was the same through the study interval (1950-2014). Given that we had no way to test the validity of this assumption, and to ensure it did not fundamentally alter geodetic mass balance results, we also computed results for the truncated glacier (Table S1, Supplement). The difference between the truncated and infilled geodetic mass balance was ≤0.04 m w.e. yr^{-1} for both 1950-1960 and 1960-2005 (Table S2, Supplement), which is less than the accounted geodetic

mass balance error (0.05 m w.e. yr^{-1} for 1950-1960, 0.12 m w.e. yr^{-1} for 1960-2005). Infilling data for the missing upper section therefore does not alter geodetic mass balance results beyond the reported uncertainty bounds.

3.4 Glaciological mass balance

Sperry Glacier has been the focus of a United States Geological Survey (USGS) intensive glacier mass balance monitoring program since 2005. Therefore, glaciological mass balance measurements of seasonal mass gains and losses at Sperry Glacier are available from the year 2005 onward (Clark et al., 2017). We used these data, measured in the field according to standard mass balance protocols (Kaser et al., 2003; Ostrem and Brugman, 1991) to define specific, conventional (Cogley et al., 2011) winter and summer glacier mass balance from 2005-2014. We also analyzed point balance data collected along a longitudinal transect to inspect mass balance gradients at Sperry Glacier. To correct for bias in the raw, specific glaciological balances reported by Clark et al. (2017), we performed calibration as outlined by Zemp et al. (2013). The results of this calibration, which utilized the 2005-2014 geodetic mass balance calculated in this study, are reported in Table 1.

3.5 Mass balance and climate regressions

Employing annual glaciological measurements (Clark et al., 2017), we defined a functional relationship (i.e. linear regression) between 2005-2014 specific surface mass balance and regional climate. Regional climate was defined by meteorological data on winter peak snow water equivalent (SWE) and summer positive degree days (PDD). Meteorological data from 2005-2014 were used to define the regressions, and meteorological data from 1950-2005 were used to apply the regressions back in time.

3.5.1 Meteorological and snow data

The Global Historical Climatology Network (HCN) provides historic temperature data for Kalispell, Montana located approximately 50 km southwest of Sperry Glacier. There are closer meteorological stations, but these had short and incomplete records. For example, average daily temperatures were recorded at Sperry Glacier for most (83%) summer days from 2005-2013. We used this shorter, discontinuous record to vet the longer, continuous Kalispell record. The Kalispell HCN record reports continuous daily average air temperatures back to 1950 for the melt season summer months, defined as July, August, and September (Clark et al., 2017). However, Kalispell is located at 901 m, which is 1554 m lower than the average elevation across Sperry Glacier in 2005-2014. We therefore applied a lapse rate correction of 5.57 °C km^{-1}, calculated using 7 years of temperature measurements from a recently installed meteorological station at Sperry Glacier, to correct for the elevation difference. Comparison of lapse-rate-corrected temperatures derived from the Kalispell HCN meteorological station with this 7 year record of in situ July, August, September temperatures yielded no statistically significant difference at the 99% confidence interval (p<0.01), and the distribution of residuals was normal.

Because the glacier terminus increased in elevation from 1950-2014, Sperry Glacier was on average 35 m lower in elevation during 1950-1960, and 21 m lower in elevation during 1960-2005. We accounted for these changes in elevation by adjusting the lapse rate correction accordingly for each time period. The effect of this accounting was small, resulting in -0.16° and -0.12° changes to average summer temperature, and -24 ° day and -14 ° day changes to PDD. Ultimately, correcting for elevation changes at Sperry Glacier corresponded to cm-scale changes to the mass balance regression (Fig. S2, Supplement).

Data from the Natural Resources Conservation Service at five nearby snow course sites (Desert Mountain, 1707 m; Piegan Pass, 1676 m; Marias Pass, 1600 m; Mount Allen, 1737 m; and Mineral Creek, 1219 m) and one adjacent Snow Telemetry (SNOTEL) site (Flattop Mountain, 1921 m) provide SWE data for locations within a 50 km radius of Sperry Glacier (Fig.1a). SWE is recorded monthly at snow course sites, via manual measurement, whereas SWE is recorded daily at SNOTEL sites via transducer measurements from a snow pillow.

We analyzed the historical snow data from the region against observations from Sperry Glacier, and found high correlation coefficients ($r^2 \geq 0.939$) for each of the seven datasets analyzed (Table S3, Supplement). The highest correlation was with Flattop Mountain SNOTEL ($r^2 = 0.990$), but at this station consistent snow data only go back to 1970. The second highest correlation ($r^2 = 0.973$), for a snow record that started prior to 1950 and so encompassed the geodetic record, was Mount Allen. We therefore used Mount Allen snow data for our mass balance regression.

3.5.2 Regression analysis

To quantify the glacier-climate relationship for 2005-2014, we fit a linear regression between 2005-2014 meteorological (x: PDD, SWE) and glaciological mass balance (y: b_s, b_w) data. We forced the best-fit line through the origin so that zero PDD and zero SWE equated to zero melt and zero accumulation, respectively. The linear combination of the two seasonal linear equations was thus:

$$B_a = m_s\,(PDD) + m_w(SWE) \tag{5}$$

where B_a is the specific annual balance, m_s is the summer proportionality factor, m_w is the winter proportionality factor, PDD is summer positive degree days, i.e. the sum of the average temperatures of days above 0 °C during the melt season, and SWE is peak winter snow water equivalent. We solved for the proportionality factors using an ordinary least squares, one parameter linear regression.

The linear regression only provides a best estimate of the mass balance of Sperry Glacier. To discern how dependable this estimate was, we considered the 95% confidence interval on each seasonal linear regression. Knowing that the true proportionality factor (i.e. slope of the best fit line) fell somewhere within the upper and lower bounds, we used the upper and lower confidence intervals to compute maximum and minimum possible mass balances. This accounting accommodated

uncertainty due to (a) the discrepancy between snow and meteorological station locations and Sperry Glacier, (b) assuming that seasonal melt is largely driven by net available shortwave radiation and that PDD is a reasonable proxy for this, and (c) assuming that the summer melt season is limited to July, August, and September.

3.6 Shading, avalanching, and wind-drifting

To assess topographic shading, we used the Solar Area Radiation tool (ESRI, 2014) to calculate cumulative insolation received across Sperry Glacier during the melt season months of July, August, and September in 2014, when the glacier was smaller, steeper, and more shaded, versus 1950, when the glacier was larger, flatter, and less shaded. This hemispherical viewshed algorithm (Fu and Rich, 2002) calculated insolation based on an upward-looking sky map for every grid cell within our 2014 DEM, the seasonal progression of the position of the sun relative to Earth, a fixed atmospheric transmissivity, topographic shading, latitude, elevation, slope, and aspect. To qualitatively assess avalanching and wind-drifting snow processes, we examined field observations, historic photographs, and field-measured mass balance data collected by Clark et al. (2017).

4 Results

4.1 Retreat, thinning, and negative mass balance

Sperry Glacier has decreased from 1.30 km^2 in 1950, to 1.23 km^2 in 1960, to 0.86 km^2 in 2005, to 0.80 km^2 in 2014 (Table 1). During the mid-20th century the glacier extended onto relatively flat (<15° slope) bedrock terrain, therefore the lower portion of the glacier was relatively low angle. As a result, between 1950 and 2014, despite nearly 0.5 km of retreat, the glacier terminus only receded upward by 56 m in elevation. The loss of this northeast-oriented, low-sloping terminus resulted in a steepening of the glacier's average slope by 7 ^{0}, and a rotation of the glacier's average aspect toward the north by 24 ^{0}.

Elevation change across the glacier surface is generally similar in its spatial pattern, but not magnitude, during 1950-1960, 1960-2005, and 2005-2014 (Fig. 3a, c, e). Thinning occurred across the lower portion, but is most pronounced at the terminus. The upper elevations of the glacier thickened from 1960-2005 and 2005-2014, but at rates less than +1 m yr^{-1} (Fig. 3). The magnitude of thinning near the terminus is distinct for each period. Terminal thinning rates from 1950-1960 were up to -2.5 m yr^{-1} (Fig. 3b), whereas terminal thinning rates from 1960-2005 (Fig. 3d) and 2005-2014 (Fig. 3f) were smaller than -1.5 m yr^{-1}. The magnitude of thickening was likewise distinct between periods, with 1950-1960 showing a bulge near the glacier's middle (approximately 2500 m), growing at nearly +1 m yr^{-1} (Fig. 3b).

Despite differences in the magnitude of elevation change, the hypsometry of the glacier remained similar in 1950, 1960, 2005, and 2014. Sperry Glacier lost 50 m of ice at the glacier terminus during the 1960-2005 interval which agrees with the average amount of thinning (52.4 m) reported for glaciers in the Canadian Rockies for the same period (Clarke et al., 2013).

5 Commensurate with its area loss and thinning, the glacier also lost volume. Geodetic mass balance results show Sperry Glacier shrank by -3.33 million m^3 from 1950-1960, -11.3 million m^3 from 1960-2005, and -0.90 million m^3 from 2005-2014. It lost -2.83 billion kg of mass from 1950-1960, -9.68 billion kg from 1960-2005, and -0.76 billion kg from 2005-2014 (Table 1). The rate of mass loss at Sperry Glacier was -0.22 ± 0.12 m w.e. yr^{-1} from 1950-1960, -0.18 ± 0.05 m w.e. yr^{-1} from 1960-2005, and -0.10 ± 0.03 m w.e. yr^{-1} from 2005-2014 (Table 2). The glacier is near balance, but slightly losing mass.

4.2 Glacier-climate relationship

10 Linear regressions show strong (r^2 > 0.97), statistically significant (p < 0.03) correlation between meteorological and glaciological data (Fig. 4). The model therefore effectively defines a functional relationship between glacier mass balance and regional climate for 2005-2014. The regressions correlate warmer summers to more negative summer mass balance (r^2 = 0.978), and snowier winters to more positive winter mass balance (r^2 = 0.973). The proportionality factor for winter (m_w), which scales snow course data on peak SWE to winter glaciological measurements, is 2.99. The proportionality factor for 15 summer (m_s), which scales meteorological data on PDD to summer glaciological measurements, is -0.004 m w.e. °C^{-1} · day^{-1}.

We used meteorological time series data to apply the linear regression back in time to 1950 (Figure 5). Average PDD during 1950-1960 was 709 ± 53 °C ·day, which was virtually the same as average PDD during 1960-2005 (717 ± 86 °C · day). Summer PDD then showed a 41 °C · day increase to an average of 758 ± 75 °C · day during 2005-2014, although this increase was well within interannual variability. Snow data show that on average, SWE decreased from 1.31 ± 0.26 m w.e. in 20 1950-1960, to 1.08 ± 0.32 m w.e. in 1960-2005, to 0.95 ± 0.25 m w.e. in 2005-2014, although these step decreases are likewise within the range of interannual variability. Generally, PDD and SWE in 1950-1960 compared to 2005-2014 seem to differ. To quantitatively assess the difference, we performed simple t-tests. T-test results showed that the lower average SWE during 2005-2014 differed statistically from 1950-1960 SWE with (p < 0.01, α = 0.99), and higher PDD (p < 0.15, α = 0.85). This evidence supports the notion that 2005-2014 had relatively warm summers and dry winters compared to 1950-25 1960.

Nevertheless, geodetic results show that average mass change rates at Sperry Glacier for 2005-2014 and 1950-1960 were comparable (Table 3), showing mass loss rates at less than 0.25 m w.e. yr^{-1}. This differs drastically from mass balance results derived from the regression, which include many years of net mass gain during the mid-20th century (Fig. 6). Enough years are positive that the averages from 1950-1960 and 1960-2005 are positive, at +0.98 ± 0.83 m w.e. yr^{-1} and +0.34 ± 0.75 m 30 w.e. yr^{-1} respectively. However, confidence intervals from the linear regression model suggest the possibility of a negative average during 1960-2005. Conversely, error on the 1950-1960 mass balance include only positive averages, i.e. glacier

thickening and mass gain. The 1950-1960 mass gain predicted by the regression (+0.98 ± 0.83 m w.e. yr^{-1}) is distinctly at odds with the 1950-1960 geodetic mass balance of -0.22 ± 0.12 m w.e. yr^{-1}.

4.3 Local controls on surface mass balance

The amount of potential clear sky radiation available for specific summer melt at Sperry Glacier decreased by 118,605 kJ m^{-2}
(approximately 30%) from 1950-2014, likely due to steepening of the glacier surface, and a greater proportion of the glacier becoming shaded. Given the heat of fusion for ice (334 kJ m^{-2}), this energy deficit translates to 0.36 m w.e. less potential melt, driven only by changes in the relative influence of local effects (i.e. shading, steepening), independent of climate. Field observations show that the rock headwall extending above Sperry Glacier (Fig. 2) contributes high frequency, low volume, loose avalanches (Fig. 7a), and that the cornice above the bergschrund often breaks in the spring, subsequently triggering localized slab avalanches which extends 500 m down from the crest of the ridge to an elevation of 2460 m. (Fig. 7b). Historic aerial photographs show that a prominent ridge of wind-drifted snow consistently develops at lower elevations in the basin (Fig. 8). Field-measured mass balance data also show evidence of wind effects on accumulation in the winter is highly variable. Accumulation ranges from 0.00 m w.e. in wind scoured areas, where seasonal snowpack had been stripped down to bare ice, up to more than 5 m w.e. in wind loaded areas (Clark et al., 2017).

Field-measured data, taken along stakes from the terminus toward the headwall of the glacier (Clark et al., 2017), show the impact of these local effects (shading, avalanching, wind drifting) on the mass balance elevation gradient (Fig. 9). Toward the glacier terminus, at elevations lower than 2475 m, the lapse rate of winter accumulation is 10×10^{-4} m w.e. (m)$^{-1}$. Toward the glacier head, at elevations above 2475 m, the lapse rate of winter accumulation is an order of magnitude higher at 150×10^{-4} m w.e. (m)$^{-1}$. The elevation gradients shown by summer ablation measurements show a similar inflection (Fig. 9). At elevations higher than 2475 m, where the glacier is steeper and more shaded, the melt lapse rate increases eightfold from 6.6×10^{-4} m w.e. (m)$^{-1}$ to 53×10^{-4} m w.e. (m)$^{-1}$.

5 Discussion

Our results reveal that the drivers of mass balance at Sperry Glacier evolved as the glacier retreated. Specifically, the strong correlation between modern-era field and geodetic mass balance poorly predicts the 1950-1960 geodetically derived mass balance (Fig. 6) suggesting a change in the relationship between regional climate and rates of ice mass loss. Viewed another way, geodetic results compared to regional climate data show that Sperry Glacier lost less area-averaged mass from 2005-2014 (-0.10 ± 0.03 m w.e. yr^{-1}) than from 1950-1960 (-0.22 ± 0.12 m w.e. yr^{-1}) despite the 2005-2014 period being characterized by warmer summers and lower precipitation winters. This study documents that the climate representativeness of Sperry Glacier has changed, as the glacier seemingly became less sensitive to regional climate as it retreated. We therefore explore the possibility that local, topographically driven mass balance effects became relatively more dominant over time compared to regional climate influence.

Unlike at many glaciers where the elevation gradient of mass balance is relatively uniform (e.g. Thomson et al., 2017), the mass balance gradient at Sperry Glacier has two distinct components reflecting regional and local drivers (Fig. 9). For example, the winter mass balance gradient at elevations below 2475 m, 10×10^{-4} m w.e. (m)$^{-1}$, falls within the range of regional SWE lapse rates, 6.2-10.4×10^{-4} m w.e. (m)$^{-1}$, reported in a study of snow accumulation in northwest Montana

5   (Gillan et al., 2010). The stark increase (to 150×10^{-4} m w.e. (m)$^{-1}$) in winter mass balance gradient at higher elevations is consistent with enhanced snow accumulation reported for so-called "drift" glaciers located below the regional equilibrium line in Colorado, where winter accumulation from local effects was four to eight times regional snow accumulation (Outcalt and MacPhail, 1965). A sudden steepening of summer mass balance gradient also exists at the top of the glacier (Fig. 9).

We ran experiments to assess the impact of the time-changing glacier hypsometry and the local and regional mass balance

10   gradients on the glacier's total mass balance. We applied field-measured mass balance gradients to the hypsometry of Sperry Glacier in 2014 and 1950 (Fig. 10), first using only the regional gradient and then using the regional plus local gradients. This demonstrates that without local effects, given the 1950 glacier hypsometry, regional lapse rates predict that the annual, specific surface mass balance would be -1.04 m w.e. Similarly, without local effects, given the 2014 glacier hypsometry, regional lapse rates predict that the annual, specific surface mass balance would be -0.96 m w.e. Thus, in theory, the mass

15   balance response of the 1950 and 2014 glaciers would be roughly similar when forced only by regional climate. However, when the local mass balance gradients are applied, the balance for 1950 increased by 37% to -0.66 m w.e., and for 2014 by 57% to -0.41 m w.e.

Partitioning the increase of local effects between seasonal components, we find that the winter local gradient (i.e. the surplus in winter accumulation due to avalanching and wind loading) accounts for 79% and that the summer local gradient (i.e. the

20   mediation in summer melt due to shading) comprised 21%. Hence, local mass balance processes, particularly relating to snow accumulation, have apparently played a strong role at Sperry Glacier since 1950, and that role strengthened as the glacier retreated. This experiment supports the interpretation that the altered mass balance response we have documented, wherein the glacier had a less negative balance in 2005-2014 despite less favorable regional climate conditions, is driven by the increasing influence of local effects rather than just the changing glacier hypsometry.

25   Sperry Glacier's increasing sensitivity to local mass balance drivers is commensurate with modeled projections of future changes to cirque glaciers in the Swiss Alps. For example, although 25% of 1133 individual very small (<0.5 km^2) glaciers are projected to disappear as soon as the next 25 years, 67 glaciers (6%) are projected to maintain more than half of their area through at least 2050 (Huss and Fischer, 2016). The persistence of these select glaciers, which are located at lower elevation than the regional ELA, signals the sometimes strong influence of local mass balance drivers. Despite local effects allowing

30   some glaciers to persist for a few more decades, categorical evidence of world-wide glacier retreat in response to 20th century warming (Roe et al., 2016) suggests that local mass balance drivers do not interrupt the synchronicity of glacier response to climate change on global, century-long scales. Thus, the evolving relationship between climate and mass balance

demonstrated by Sperry Glacier reveals the complexity in interpreting glacier changes in Glacier National Park, but does not preclude the reality of a climate that is trending toward conditions that mandate glacier disappearance.

6 Conclusion

Analysis of a 64 year record of glacier mass change against climate data demonstrates the climate representativeness of Sperry Glacier is evolving through time. By assessing geodetic mass measurements, regional climate data, and field measured mass balance, we deduced that this shift in representativeness was caused by local drivers related to topography becoming increasingly influential as the cirque glacier retreated. Our results therefore emphasize the importance of accounting for spatially complex, local topographic processes in projections of 21st century mountain glacier change. These effects can exert significant and time-changing control on the mass balance of retreating cirque glaciers, are likely highly variable from glacier to glacier, and must therefore be carefully considered and treated in interpretations and projections of cirque glacier change.

7 Disclaimer

Any use of trade, product, or firm names is for descriptive purposes only and does not imply endorsement by the U.S. Government.

Data Availability. Data and python code used for the analyses reported in this paper are available at xxx.

The Supplement related to this article is available online at doi: xxx-supplement.

Competing interests. The authors declare that they have no conflict of interest.

Author contributions. CF and JH designed the analytical approach, which CF then carried out with input from DF, JM, and EP. CF prepared the manuscript with contributions from all co-authors.

Acknowledgements. This work was funded by the Climate and Land Use Change mission area of the U.S. Geological Survey. CF received funding from the Jerry O'Neal National Park Service Student Fellowship.

References

Alden, C.: Glaciers of Glacier National Park, US Dep. Inter. Washingt. DC, 48, 1914.

Carrara, P. E.: Late Quaternary Glacial and Vegetative History of the Glacier National Park Region, Montana, U.S. Geological Survey Bulletin 1902, U.S. Department of the Interior, Washington D.C., 1989.

Clark, A. M., Fagre, D. B., Peitzsch, E. H., Reardon, B. A. and Harper, J. T.: Glaciological measurements and mass balances from Sperry Glacier, Montana, USA, years 2005-2015, Earth Syst. Sci. Data, 9(1), 47–61, doi:10.5194/essd-9-47-2017, 2017.

Clarke, G. K. C., Anslow, F. S., Jarosch, A. H., Radić, V., Menounos, B., Bolch, T. and Berthier, E.: Ice volume and subglacial topography for western Canadian glaciers from mass balance fields, thinning rates, and a bed stress model, J. Clim., 26(12), 4282–4303, doi:10.1175/JCLI-D-12-00513.1, 2013.

Cogley, J. G., Hock, R., Rassmussen, L. A., Arendt, A. A., Bauder, A., Braithwaite, R. J., Jansson, P., Kaser, G., Moller, M., Nicholson, L. and Zemp, M.: Glossary of mass balance and related terms, IHP-VII Technical Documents in Hydrology No. 86, IACS Contribution No. 2, UNESCO-IHP, Paris., 2011.

DeBeer, C. M. and Sharp, M. J.: Recent changes in glacier area and volume within the southern Canadian Cordillera, Ann. Glaciol., 46, 215–221, doi:10.3189/172756407782871710, 2007.

DeBeer, C. M. and Sharp, M. J.: Topographic influences on recent changes of very small glaciers in the monashee mountains, British Columbia, Canada, J. Glaciol., 55(192), 691–700, doi:10.3189/002214309789470851, 2009.

Dyurgerov, M. B. and Meier, M. F.: Twentieth century climate change: Evidence from small glaciers, PNAS, 97(4), 1406–1411, 2000.

ESRI: ArcGIS Desktop: Release 10.3.1, 2014.

Fagre, D. B., McKeon, L. A., Dick, L. A. and Fountain, A. G.: Glacier margin time series (1966, 1998, 2005, 2015) of the named glaciers of Glacier National Park, MT, USA, U.S. Geol. Surv. data release, 2017.

Fahey, M.: National Civil Applications Program, U.S. Geological Survey, Reston, VA, USA, 2014.

Fu, P. and Rich, P. M.: A geometric solar radiation model with applications in agriculture and forestry, Comput. Electron. Agric., 37(1–3), 25–35, doi:10.1016/S0168-1699(02)00115-1, 2002.

Gillan, B. J., Harper, J. T. and Moore, J. N.: Timing of present and future snowmelt from high elevations in northwest Montana, Water Resour. Res., 46(1), n/a-n/a, doi:10.1029/2009WR007861, 2010.

Hock, R.: Temperature index melt modelling in mountain areas, J. Hydrol., 282(1–4), 104–115, doi:10.1016/S0022-1694(03)00257-9, 2003.

Hoffman, M. J., Fountain, A. G. and Achuff, J. M.: 20th-century variations in area of cirque glaciers and glacierets, Rocky Mountain National Park, Rocky Mountains, Colorado, USA, Ann. Glaciol., 46, 349–354, doi:10.3189/172756407782871233, 2007.

Huss, M. and Fischer, M.: Sensitivity of Very Small Glaciers in the Swiss Alps to Future Climate Change, Front. Earth Sci., 4(April), 1–17, doi:10.3389/feart.2016.00034, 2016.

Johnson, A.: Grinnell and Sperry Glaciers, Glacier National Park, Montana: A record of vanishing ice, Geol. Surv. Open-File Rep., 1180, 1–29, 1980.

Kaser, G., Fountain, A., Jansson, P., Heucke, E. and Knaus, M.: A manual for monitoring the mass balance of mountain glaciers, UNESCO, 137, 2003.

Kuhn, M.: The mass balance of very small glaciers, Zeitschrift fur Gletscherkd. und Glazialgeol., 31, 171–179, 1995.

Laha, S., Kumari, R., Singh, S., Mishra, A., Sharma, T., Banerjee, A., Nainwal, H. C. and Shankar, R.: Evaluating the contribution of avalanching to the mass balance of Himalayan glaciers, , 1–17, doi:10.1017/aog.2017.27, 2017.

Nuth, C. and Kääb, A.: Co-registration and bias corrections of satellite elevation data sets for quantifying glacier thickness change, Cryosphere, 5(1), 271–290, doi:10.5194/tc-5-271-2011, 2011.

5 Ostrem, G. and Brugman, M.: Glacier Mass Balance Measurements: A Manual for Field and Office Work, Minist. Supply Serv. - Environ. Canada Norweigian Water Energy Adm., 224, 1991.

Outcalt, S. J. and MacPhail, D. D.: A survey of Neoglaciation in the Front Range of Colorado, University of Colorado Press, Boulder, CO., 1965.

Roe, G. H., Baker, M. B. and Herla, F.: Centennial glacier retreat as categorical evidence of regional climate change, Nat. 10 Geosci., 10(2), 95–99, doi:10.1038/ngeo2863, 2016.

Ruiz, L., Berthier, E., Viale, M., Pitte, P. and Masiokas, M. H.: Recent geodetic mass balance of Monte Tronador glaciers, northern Patagonian Andes, Cryosphere, 11(1), 619–634, doi:10.5194/tc-11-619-2017, 2017.

Sibson, R.: A Brief Description of Natural Neighbor Interpolation, in Interpolating Multivariate Data, pp. 21–36, John Wiley & Sons, New York., 1981.

15 Thomson, L. I., Zemp, M., Copland, L., Cogley, J. G. and Ecclestone, M. A.: Comparison of geodetic and glaciological mass budgets for White Glacier, Axel Heiberg Island, Canada, J. Glaciol., 63(237), 55–66, doi:10.1017/jog.2016.112, 2017.

Zemp, M., Thibert, E., Huss, M., Stumm, D., Rolstad Denby, C., Nuth, C., Nussbaumer, S. U., Moholdt, G., Mercer, A., Mayer, C., Joerg, P. C., Jansson, P., Hynek, B., Fischer, A., Escher-Vetter, H., Elvehøy, H. and Andreassen, L. M.: Reanalysing glacier mass balance measurement series, Cryosphere, 7(4), 1227–1245, doi:10.5194/tc-7-1227-2013, 2013.

20 Zemp, M., Frey, H., Gärtner-Roer, I., Nussbaumer, S. U., Hoelzle, M., Paul, F., Haeberli, W., Denzinger, F., Ahlstrøm, A. P., Anderson, B., Bajracharya, S., Baroni, C., Braun, L. N., Cáceres, B. E., Casassa, G., Cobos, G., Dávila, L. R., Delgado Granados, H., Demuth, M. N., Espizua, L., Fischer, A., Fujita, K., Gadek, B., Ghazanfar, A., Hagen, J. O., Holmlund, P., Karimi, N., Li, Z., Pelto, M., Pitte, P., Popovnin, V. V., Portocarrero, C. A., Prinz, R., Sangewar, C. V., Severskiy, I., Sigurðsson, O., Soruco, A., Usubaliev, R. and Vincent, C.: Historically unprecedented global glacier decline in the early 21st 25 century, J. Glaciol., 61(228), 745–762, doi:10.3189/2015JoG15J017, 2015.

Zhang, B.: Towards a higher level of automation in softcopy photogrammetry: NGATE and LiDAR processing in SOCET SET®, in GeoCue Corporation 2nd Annual Technical Exchange Conference, p. 32, Nashville, Tennessee., 2006.
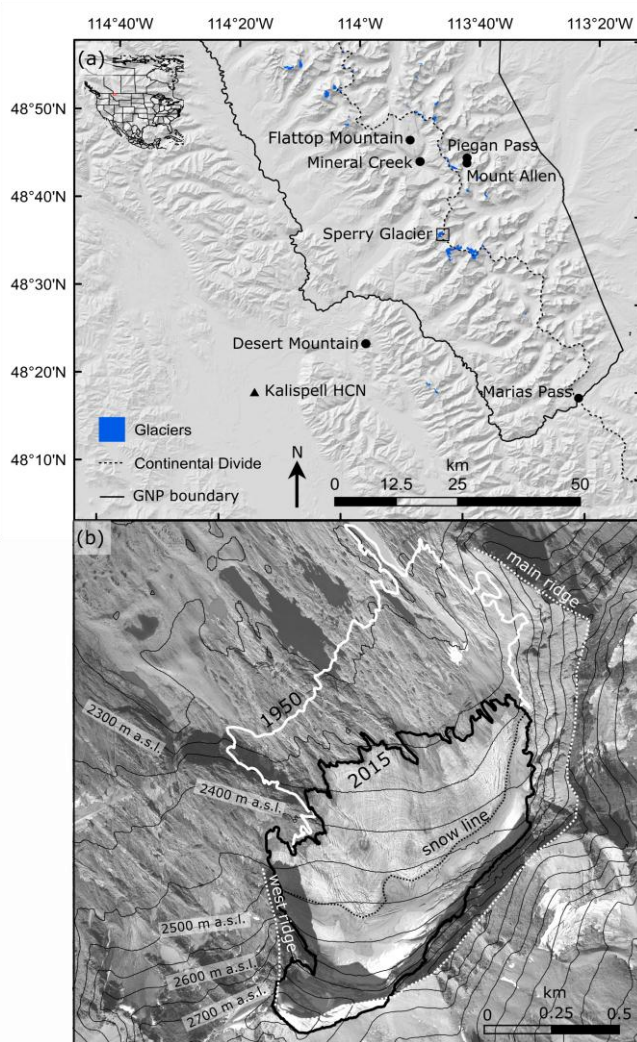
Figure 1: (a) Study area in the U.S. Northern Rocky Mountains, located just south of the USA-Canada border, as indicated by the red box on the inset map. The 39 named glaciers within and near Glacier National Park (GNP) are shown (blue). The continental divide (dashed black line), GNP boundaries (solid black line), the location of Sperry Glacier (small box), meteorological station (black triangle), and snow measurement sites (black circles), are also shown. (b) Aerial image depicts Sperry Glacier in 2015 with the 1950 (white line) and 2014 (black line) glacier margins shown. The seasonal snow line (dotted black line) and the main ridge that defines the crest of the cirque headwall above Sperry Glacier, as well as the west ridge which bounds Sperry Glacier (dotted white line), are also depicted. Elevation (m) is represented by thin black contour lines.
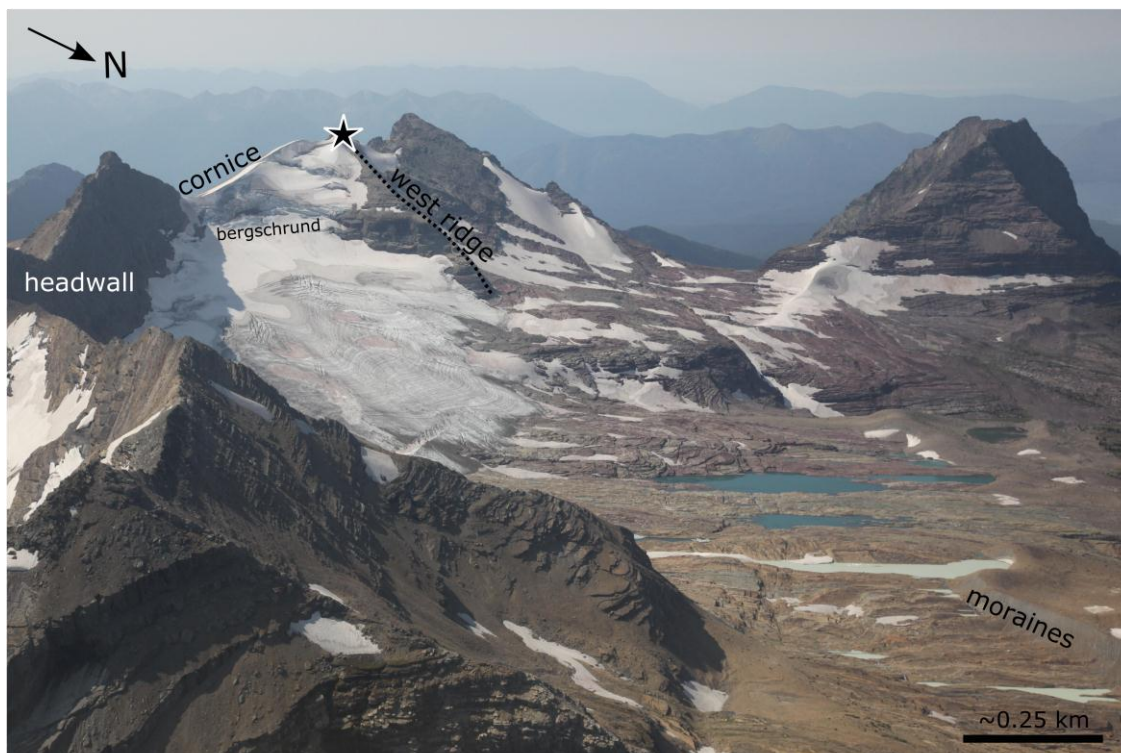
Figure 2: Sperry Glacier on 01 September 2009. Arrow points to the north. Note low-sloping proglacial terrain. In 1950 and 1960, the glacier extended onto this relatively flat ground. Gunsight Peak is indicated by the black star. The west ridge, headwall, cornice, bergschrund, and moraines discussed in the text are labeled. Photograph credit: Jon Scurlock.
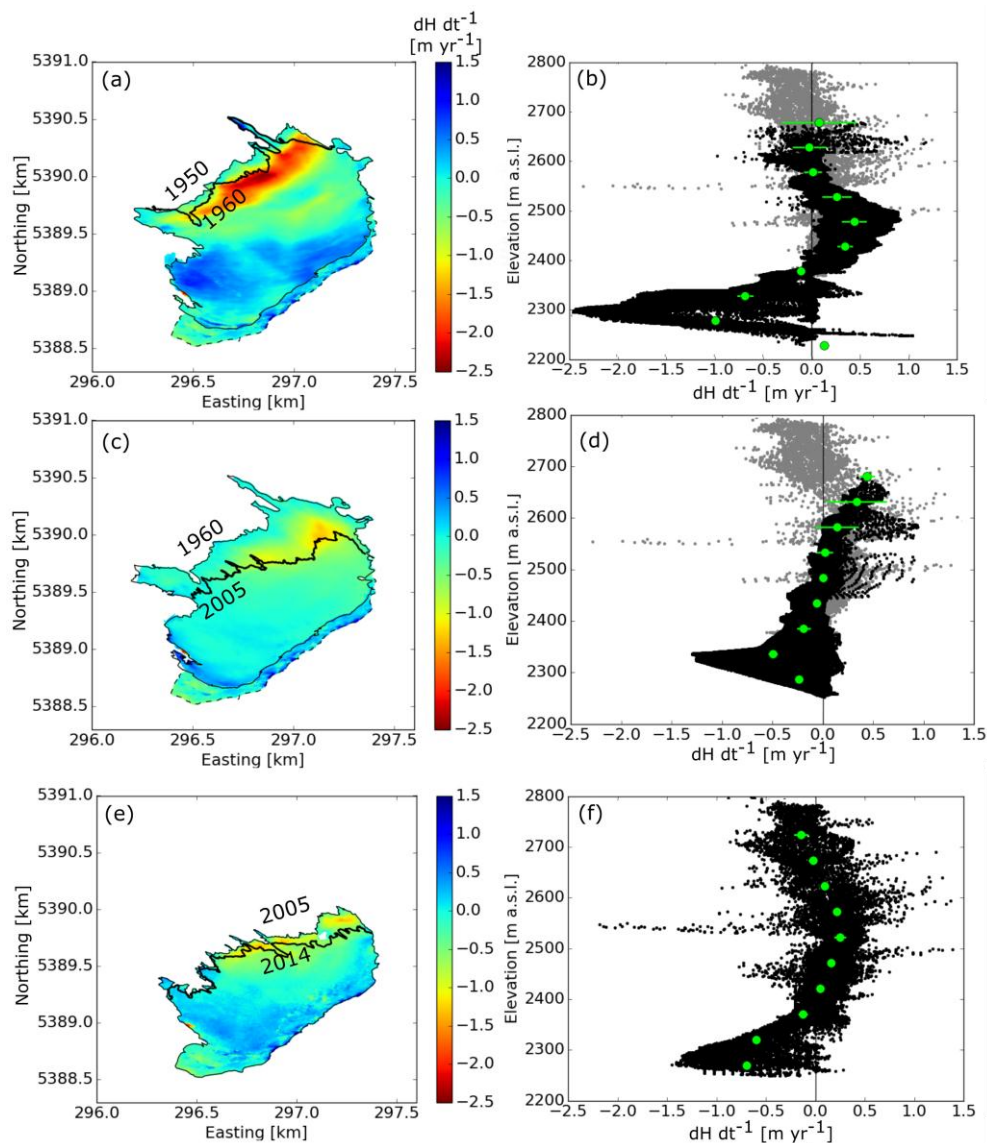
Figure 3: Elevation change over Sperry Glacier from (a,b) 1950-1960, (c,d) 1960-2005, and (e,f) 2005-2014. Left column shows elevation change across the glacier surface, and right column shows hypsometry of elevation change. Black dots on the hypsometry figures (b,d,f) indicate individual pixels, green dots indicate elevation band means, and horizontal green bars indicate elevation band mean errors. Error is mostly smaller than, and therefore obscured by, the green dot. The missing upper section is delineated by the dotted line in (a) and (c). Data from 2005-2014 were used to fill in this missing section. These 2005-2014 infill data are indicated by the gray dots in (b) and (d).
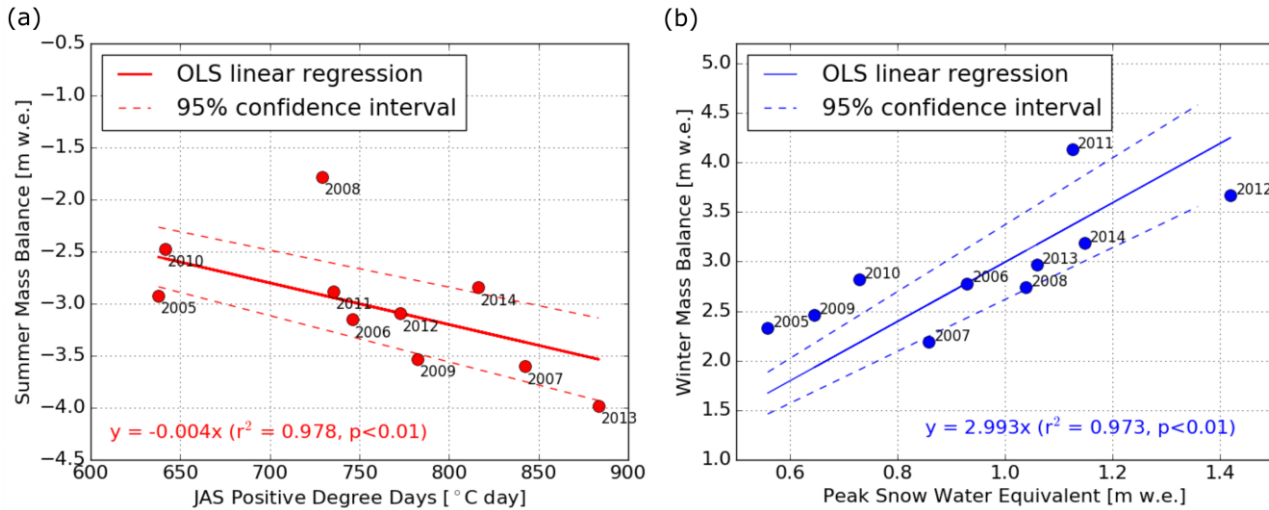
Figure 4: Ordinary least squares linear regressions between meteorological data and glaciological mass balance for 2005-
2014. (a) Summer, i.e. July, August, September (JAS), positive degree days versus summer mass balance. The linear
regression is shown in red text (y = -0.004 x) and is plotted (solid red line). The 95% confidence interval on the regression is
also shown (dotted red lines). The one parameter regression explains 97.8% of the variability ($r^2 = 0.978$) and is statistically
significant ($p < 0.01$) although the sample is small (n = 9). (b) Peak snow water equivalent versus winter mass balance. The
linear regression is shown in blue text (y = 2.99x) and is plotted (sold blue line). The 95% confidence interval on the
regression is also shown (dotted blue lines). The one parameter regression explains 97.3% of the variability ($r^2 = 0.973$) and is
statistically significant ($p < 0.01$) although the sample is small (n = 9).
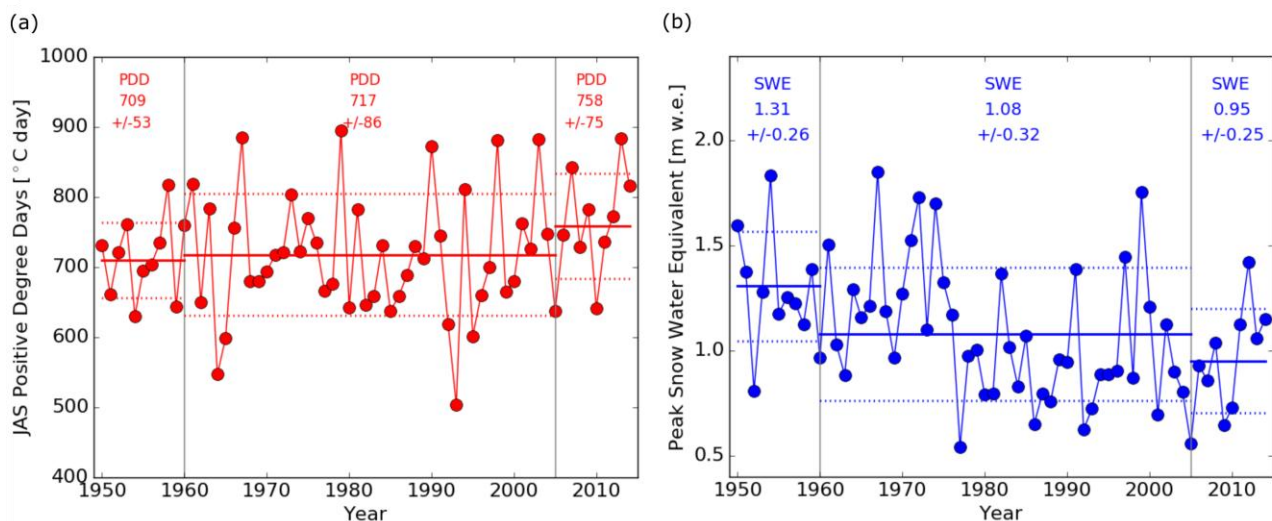
Figure 5: Meteorological time series data for 1950-2014. (a) Positive degree days (PDD) calculated from the Kalispell Historical Climate Network summer, i.e. July, August, September (JAS), temperature data, adjusted for elevation by the standard lapse rate. (b) Peak snow water equivalent (SWE), calculated from Mount Allen snow course data. Mean (solid line) and one standard deviation (dashed line) of PDD and SWE for each geodetic mass balance interval (1950-1960, 1960-2005, 2005-2014) are plotted and reported in text with standard deviation.
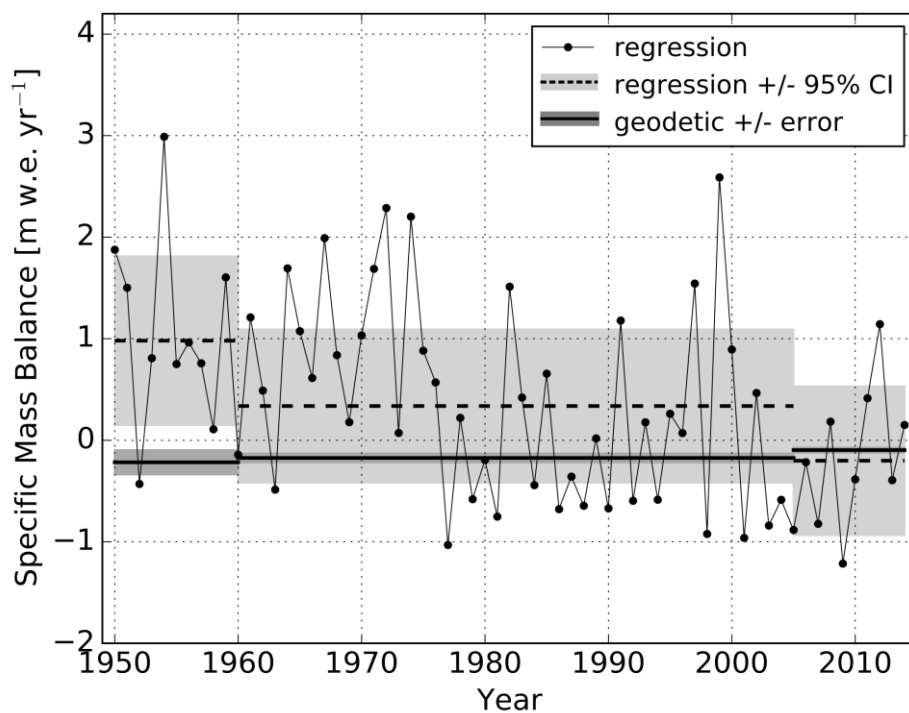
Figure 6: Comparison of regression and geodetic mass balance results. Regression results for annual mass balance (black dots, thin black line) are shown, as are regression results for the average mass balance from 1950-1960, 1960-2005, 2005-2014 (black dotted lines). Errors, set by confidence intervals on the linear regression, are also shown (light gray boxes).

5   Geodetic mass balances for 1950-1960, 1960-2005, and 2005-2014 are plotted (horizontal black lines) with errors (dark gray boxes).
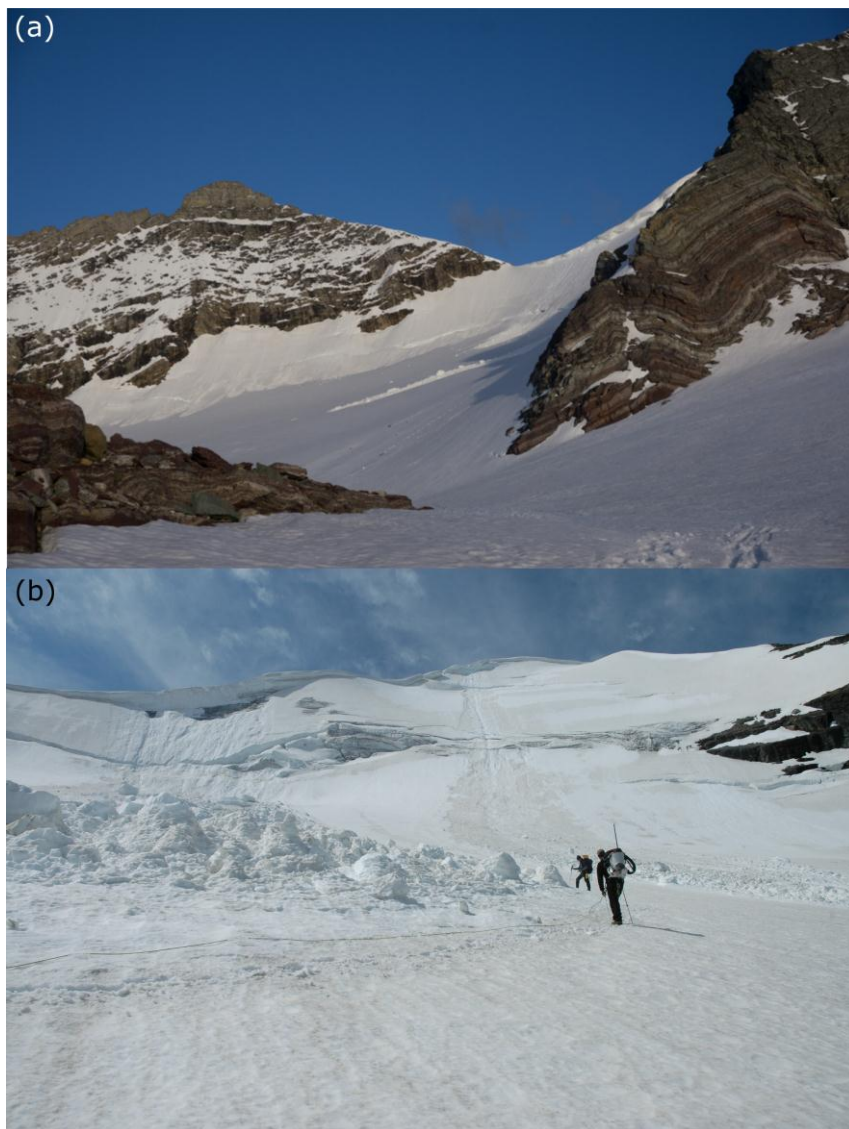
Figure 7: Snow avalanches at Sperry Glacier. (a) Sperry Glacier in June, 2010. Snow sluffing and loose avalanches off the headwall are depicted. Photo source: Joel Harper. (b) Sperry Glacier in June, 2006. Cornice collapse (on the left) often causes a localized slab avalanche. Loose avalanche depicted on the right. Photograph credit: USGS Climate Change in Mountain Ecosystem photograph archives.
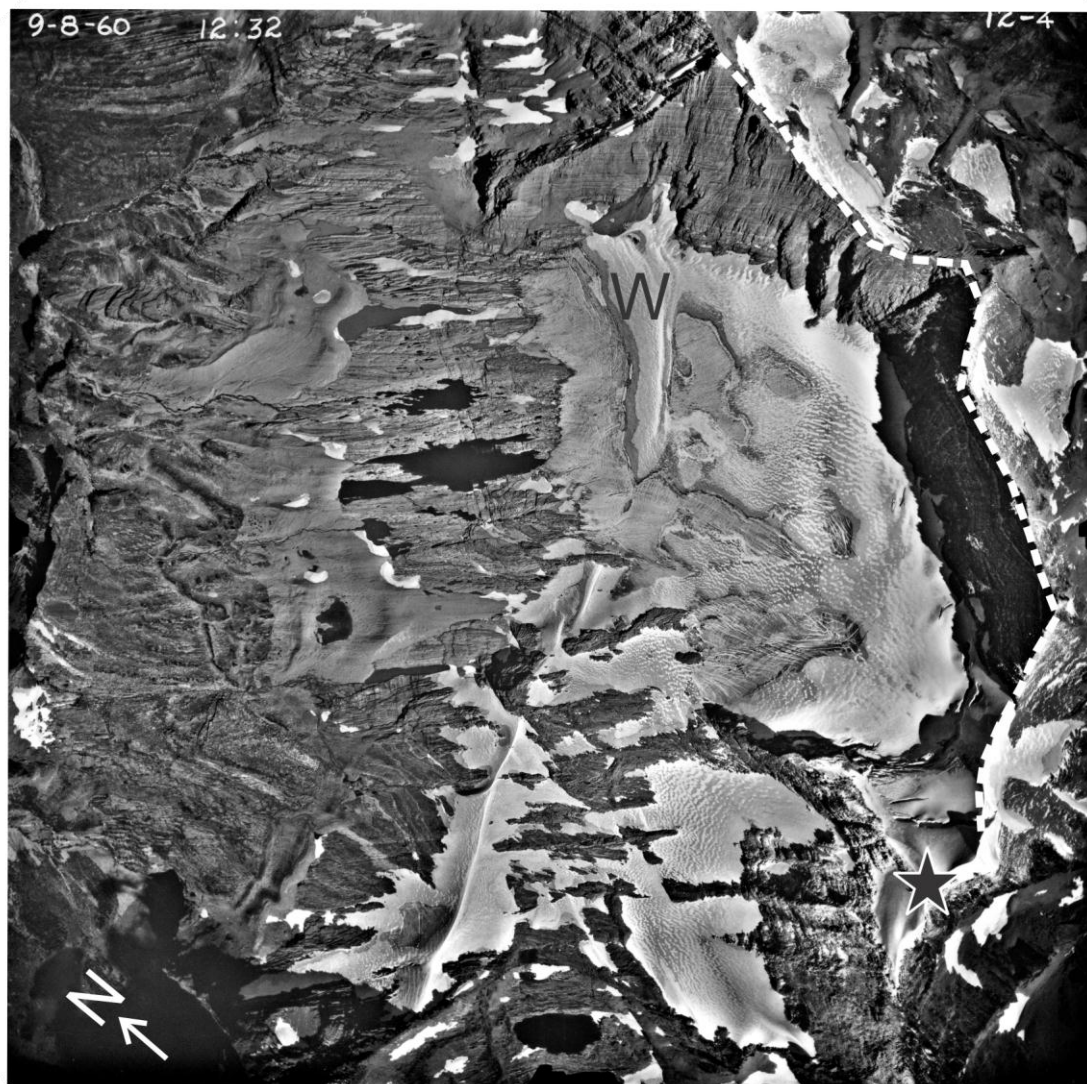
Figure 8: Aerial photograph of Sperry Glacier taken on 8 September 1960 shows a prominent ridge of wind drifted snow (W), and shows the glacier lapping over the top of Gunsight Peak (black star) at the highest elevation of the ridge (dotted white line). Photograph credit: USGS Climate Change in Mountain Ecosystem photograph archives.
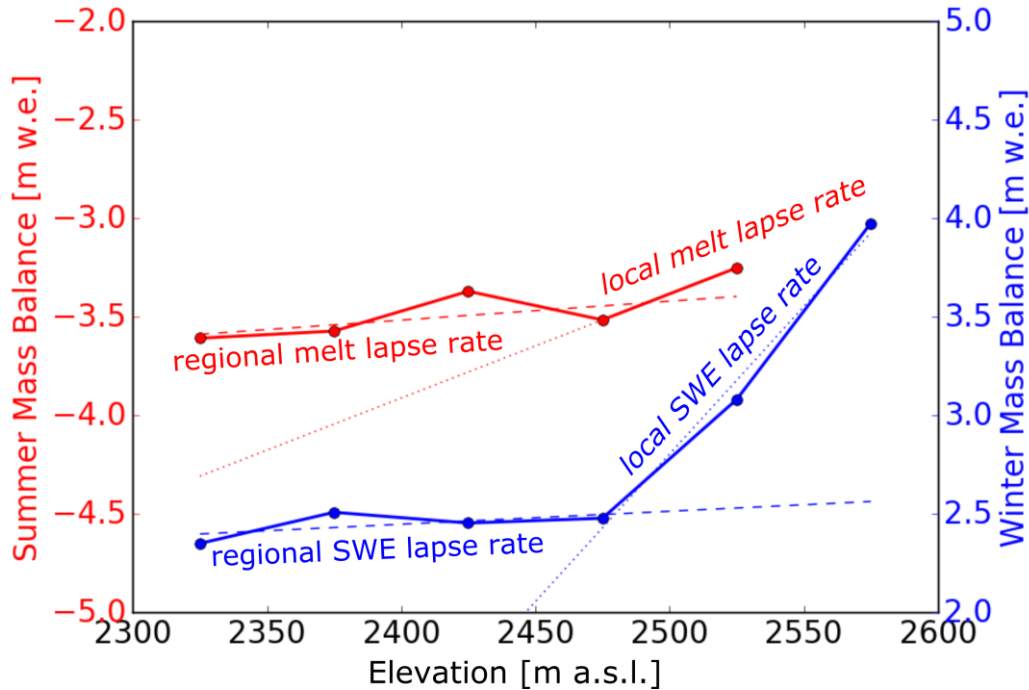
Figure 9: Mass balance gradients measured at Sperry Glacier. Data plotted are the mean of 2005-2014 measurements recorded at in-situ mass balance stakes from Clark et al. (2017). The mean of 2005-2014 summer (red dots/solid red line) and winter (blue dots/solid blue line) point mass balances, measured at stakes sites, are plotted against the average elevation of the 50 m elevation band wherein the stake was located. Linear lapse rates fit to these data are also plotted. Lower elevation (< 2475 m) mass balance gradients reflect regional lapse rates for melt (dashed red line) and SWE (dashed blue line). Higher elevation (> 2475 m) gradients reflect local lapse rates for melt (dotted red line) and SWE (dotted blue line).
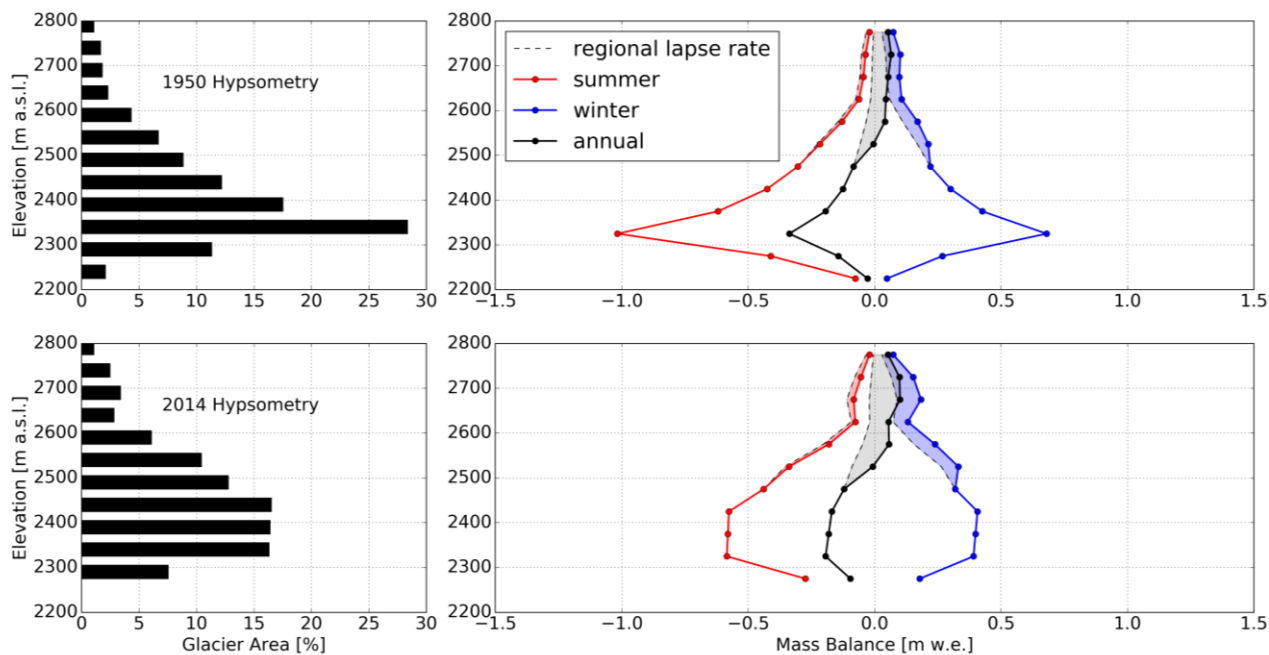
Figure 10: Parsing local from regional mass balance drivers. (a) Hypsometry of the 1950 glacier, presented in 50 m elevation bands. (b) Sperry Glacier mass balance, as it varies with elevation, given 1950 glacier hypsometry and the mass balance gradients measured by 2005-2014 stake balance data (Clark et al, 2017). Solid lines show the summer (red), winter (blue), and annual (black) balances. Dotted black lines show the same but excluding local lapse rates at high elevations, i.e. using regional lapse rates only. The difference between the solid and dotted lines highlights the effect of local controls on mass balance: suppression of summer melt (light red area), surplus in winter accumulation (light blue area), and net mass balance enhancement (light gray area). (c) Hypsometry of the 2014 glacier surface. (d) Sperry Glacier mass balance as shown in (b), but given 2014 glacier hypsometry.

Table 1: Area-averaged glaciological mass balance values used in this study. Winter balances are as reported by Clark et al. (2017). Summer and annual balances are the result of calibration against the 2005-2014 geodetic mass balance, accomplished following the method outlined by Zemp et al. (2013).

	Summer Balance (m w.e.)	Winter Balance (m w.e.)	Annual Balance (m w.e.)
2005	-3.01	+2.33	-0.68
2006	-3.36	+2.78	-0.58
2007	-3.54	+2.19	-1.35
2008	-1.60	+2.74	+1.14
2009	-3.68	+2.46	-1.22
2010	-2.50	+2.82	+0.32
2011	-3.13	+4.13	+1.00
2012	-3.09	+3.67	+0.58
2013	-3.87	+2.97	-0.90
2014	-2.95	+3.19	+0.24

Table 2: Digital elevation model (DEM) specifications and glacier elevation results. Acquisition dates for the original imagery used to derive elevation data are listed.

	DEM Source	Area (km^2)	Mean Elevation (m)	Mean Slope (°)	Mean Aspect (°)
01 Sept 1950	USGS Topographic Map 1:6,000	1.30	2402	17	336 NNE
08 Sept 1960	USGS Topographic Map 1:6,000	1.23	2408	19	340 NNE
02 Sept 2005	National Technical Means Imagery	0.86	2445	22	313 NE
07 Sept 2014	National Technical Means Imagery	0.80	2466	24	312 NE

Table 3: Geodetic mass balance results. Net changes in volume (ΔV) and mass (ΔM) on Sperry Glacier from 1950-1960, 1960-2005, and 2005-2014 are listed. Uncertainties due to elevation error (EΔh) and density (Eρ) are listed, as are total errors (E_t). Geodetic mass balances (dH dt^{-1}) are listed with uncertainty defined by total error, expressed as a rate.

	Net Volume Change	Net Mass Change	Elevation Error	Density Error	Total Error	Geodetic Mass Balance
	ΔV	ΔM	EΔh	Eρ	E_t	dH dt^{-1}
	(m^3 x 10^6)	(kg x 10^9)	(m w.e.)	(m w.e.)	(m w.e.)	(m w.e. yr^{-1})
1950-1960	-3.33	-2.83	1.20	0.18	1.22	-0.22 ± 0.12
1960-2005	-11.3	-9.68	2.16	0.68	2.27	-0.18 ± 0.05
2005-2014	-0.90	-0.76	0.26	0.06	0.27	-0.10 ± 0.03